ON THE NUMERICAL SIMULATION OF POWDER COMPACTION PROCESSES: POWDER TRANSFER MODELLING AND CHARACTERIZATION

J. C. Cante, J. Oliver, C. González, J. A. Calero and F. Benítez

Dr. J. C. Cante
Technical University of Catalonia (UPC)
Campus Terrassa, TR45
C/. Colom, 11, 08222 Spain
e-mail: juan.cante@upc.es

Prof. J. Oliver
International Center for Numerical Methods in Engineering (CIMNE)
Technical University of Catalonia (UPC)
Campus Nord UPC, Edifici C1
Jordi Girona 1-3, 08034 Barcelona, Spain
e-mail: xavier.oliver@upc.es

C. González
International Center for Numerical Methods in Engineering (CIMNE)
Campus Nord UPC, Edifici C1
Jordi Girona 1-3, 08034 Barcelona, Spain
e-mail: ferrari@cimne.upc.es

Dr. J. A. Calero
AMES S. A
Crta Nal. 340 Km 1242 Pol. Ind. Les Fallulles,
08620 San Vicenc dels Horts, Spain
e-mail: jacalero@alme.ames.es

F. Benitez
AMES S. A
Crta Nal. 340 Km 1242 Pol. Ind. Les Fallulles,
08620 San Vicenc dels Horts, Spain
e-mail: fbenitez@alme.ames.es

Abstract

A numerical model for the powder transfer stage in powder metallurgy cold compaction processes, and the corresponding material characterization procedure, are proposed. They have been designed on the basis of the following requirements: a) robust and consistent computational mechanics ingredients, b) reliability of the obtained results for practical processes in powder metallurgy and, c) industrial viability in the sense that characterization of any mixture doesn't require either much effort or much time to the end-user. The starting point is a previously developed numerical model for powder compaction, formulated in terms of the large plastic deformation theory, which requires calibration of four parameters controlling the evolution of the yield surface. This calibration, which had been successfully carried out in the past in the range of moderate to high densities, is now extended to very low densities in order to make numerical simulations able to deal with compaction processes involving relevant powder transfer stages. To circumvent the difficulties inherent to direct measurements of very low powder densities, a simple apparatus, which allows studying the powder motion in the chamber, has been designed to provide an indirect way of calibration. On this basis, a set of calibration experiments is proposed.

The proposed methodology appears to be simple and industrially viable. Although in the work it is applied to the specific constitutive model used by the authors, it appears also available for other families of constitutive models for powder compaction. As a relevant result, this would allow the same constitutive model to be used, via only the appropriated material characterization, for simulation of densification in powder transfer stages as well as in pure compaction stages.

1. INTRODUCTION

During the last two decades, a number of numerical models to predict the mechanical behaviour of the powder during compaction processes[1-10] have been proposed. Their mechanical (constitutive) ingredients are, in general, particularizations of the family of porous and frictional elasto-plastic material models, including one or more yield surfaces, with either associative or non-associative flow rules, and several (density dependent) parameters that control the size and shape of the yield surface.

As for the numerical strategy, the Finite Element Method has been successfully applied to powder forming simulation[2,5-7,10-11,16-17] but essentially restricted to the pressing and ejection phases. In these cases a full die cavity, with the required amount of properly distributed powder of uniform density, is taken as the initial geometry for the simulation of the subsequent compaction process. However, this assumption is not valid for the actual manufacturing process of a great variety of industrial parts that exhibit different levels on the upper face. Although during the filling stage the feeder moves over the die cavity producing a flat powder surface, then, and prior to the compaction phase, a powder transfer stage, achieved through repositioning of the tooling elements, takes place. In this stage, powder particles experience substantial motions, which can result in relevant densifications in certain zones that cannot be neglected for the rest of the simulation.

Friction among the powder grains, tooling kinematics and, occasionally, the applied forces are the main factors that can distort density distributions during powder transfer stages. In many cases, partially empty powder regions can appear that result in very low-density zones after compaction, which, in turn, are responsible for mechanical defects in the final part. Removal or minimization of these zones requires, among other actions, a proper definition of the tooling kinematics. Therefore, the powder transfer stage should be considered in any comprehensive numerical simulation tool aiming at helping the designer of the compaction process.

However, this transfer stage has been little analysed. The reasons are diverse: on one hand the difficulty to obtain reliable experimental results and, on the other, the important difficulties found when trying to simulate large motions of the powder with the numerical tools developed so far. From the experimental and numerical point of view, very relevant results in powder transfer can be found in[20,21]. In there, the use of the discrete element method (DEM) is proposed as an alternative to circumvent the intrinsic limitations of the classical Finite Element Method when the phenomena involve large displacements and strains.
On the contrary, the present work focuses on a generalization of the powder compaction model, initially described in[9-11], which is extended to include the powder transfer stage from a continuum point of view. Based on: a) some experimental results reported in the literature so far[14-17,20], b) a small number of parameters to be calibrated in the constitutive model and c) the computational efficiency of the resulting numerical tool, we propose in this work a multi-surface frictional like elasto-plastic constitutive model, formulated in terms of the large plastic

deformations, in which the failure envelope is a Drucker-Prager surface and the cap is defined by means of a centred elliptical one. A non-associative flow rule is defined on the failure envelope whereas an associative one is defined for the ellipse. The evolution of these surfaces is controlled by means of four parameters depending on the density. The constitutive model is completed adding up the Young's modulus and Poisson ratio whose evolution is defined in terms of the density. Friction between walls and powder is included through a Norton-Hoff type model that requires the calibration of one additional coefficient that depends on the velocity and density.
Calibration of the compaction model is carried out as follows: the two parameters defining the ellipse are calibrated through monitoring of the compaction of a very flat cylindrical part (thus minimizing wall friction effects), whereas the two parameters of the Drucker-Prager failure envelope are calibrated by means of fracture tests (i.e.: compression test and Brazilian disc test[15] appropriated to the brittle character of green compacted parts) . Friction coefficients are calibrated on thin cylindrical specimens with large aspect ratio, such that the effects of friction on powder densification are maximized. However, those tests cannot be performed for the region of low densities (ranging from the apparent density to the tap density, 3-4.0g/cm3, for iron powder) and the correct determination of powder behaviour for that region, is an open problem so far. In the remaining of this work, with the aim of improving the calibration at that range and keeping in mind the industrial application of the results, a new family of experiments at the low-density region is proposed

2 CONSTITUTIVE MODEL

The model is formulated in terms of the large plastic deformations and it is based on the results presented in[9-11] where a numerical model for the compaction stage was presented. There, one centred elliptic surface depending on two parameters was proposed. The extension presented here consists, essentially, of the reformulation of the yield surface, the plastic flow and its numerical implementation. The yield surface is extended to a multiple surface case adding up to the ellipse a new surface of the Drucker-Prager type (see Figure 1). Then, the ellipse is devised to capture the material hardening during compaction, whereas the role of the Drucker-Prager surface is to control the material mechanical failure at high densities and to account for friction effects between grains at low densities.

The adopted kinematics is based on the multiplicative decomposition of the deformation gradient tensor $\mathbf{F}$ that is decomposed into its elastic and plastic counterparts[22], $\mathbf{F} = \mathbf{F}^e\mathbf{F}^p$ and, consequently, the strain tensor admits an additive decomposition into the elastic and plastic strains $\mathbf{e} = \mathbf{e}^e + \mathbf{e}^p$. The plastic (irrecoverable) strain $\mathbf{e}^p$ is then interpreted as the loss of voids between grains during the compaction, and the elastic component $\mathbf{e}^e$ comes from the (recoverable upon unloading) particle elastic deformation.

The elastic response is described in terms of an elastic energy deformation defined by means of a quadratic function of the elastic strains. From that, the Kirchhoff stress tensor can be written in a Hooke law-like way in terms of the elastic stains $\mathbf{e}^e = \mathbf{e} - \mathbf{e}^p$:

$$\boldsymbol{\tau} = \lambda\, tr(\mathbf{e}^e) + 2\mu(\mathbf{e}^e) = \lambda\, tr(\mathbf{e} - \mathbf{e}^p) + 2\mu(\mathbf{e} - \mathbf{e}^p) \tag{1}$$

where μ and λ are the classical Lamé constants.

The strength evolution of the material is controlled by means of the two following surfaces:

$$\begin{aligned} &\Phi_1(\boldsymbol{\tau}, \rho) = q^2 + s_2^2(\rho) p^2 - [s_1(\rho) s_2(\rho)]^2 \le 0 \qquad (a) \\ &\Phi_2(\boldsymbol{\tau}, \rho) = q + b_1(\rho) p - b_2(\rho) \le 0 \qquad (b) \end{aligned} \tag{2}$$

where $q = \|dev\,\boldsymbol{\tau}\|$ is the norm of the deviatoric part of $\boldsymbol{\tau}$, $p = \frac{1}{3} tr\,\boldsymbol{\tau}$ is the mean stress and ρ stands for the powder density. Functions $\Phi_1(\boldsymbol{\tau}, \rho) = 0$ and $\Phi_2(\boldsymbol{\tau}, \rho) = 0$ define, respectively, an ellipse and a straight line in the *p*-*q* plane (see Figure 1). Parameters s_1 and s_2 determine the size and shape of the ellipse in terms of the radii r_1 and r_2 as:

$$s_1(\rho) = r_1(\rho) \quad ; \quad s_2(\rho) = \frac{r_2(\rho)}{r_1(\rho)} \tag{3}$$

Parameters $b_1(\rho)$ and $b_2(\rho)$ correspond, respectively, to the friction angle and cohesion of the Drucker-Prager failure envelope. Notice the dependence on the density ρ of parameters s_1, s_2, b_1, b_2 and, therefore, of the shape and size of both surfaces in Figure 1.

3. EXTERNAL FRICTION

Another relevant aspect of the compaction model is the friction between powder and tools (external friction). Several options are available for this modelling aspect i.e.:

a) *Dry or static friction* models (Coulomb-type friction) defined by:

$$\mathbf{t}_T = \mu_s(\rho)\, t_N \tag{4}$$

where $\mathbf{t}_T$ and t_N stand for the tangential and normal forces, respectively, and $\mu_s(\rho)$ is the (density dependent) friction coefficient, and

b) *Dynamic friction* models (Northon-Hoff type) given by:

$$\mathbf{t}_T = \mu_d(\rho, \mathrm{v})\, t_N \tag{5}$$

where the friction coefficient $\mu_d(\rho, \mathrm{v})$ depends on both the density and the relative powder/tool tangential velocity v. Both families were implemented and extensively checked. It was observed that the dynamic friction model exhibits a more robust behaviour for numerical simulations and, therefore, it was chosen as the default friction model. Further details about this topic can be found in[10, 11].

4. MATERIAL CHARACTERIZATION

The constitutive model described in Section 2 involves several material properties that have to be evaluated for every powder mixture to be considered in the simulations[12]. We shall term the procedure to determine the evolution of the material properties necessary for the model, and supplied to the *material database* of the simulation code, *characterization of the material*. One should impose to that procedure the following requirements: a) *simplicity,* in the sense that characterization of any mixture does not require either much effort or much time to the end-user b) *accuracy* of the results (in appropriate balance with the first requirement) and c) *consistency* with the selected mathematical model.

Some of the material properties involved in the model in Section 2, have an immediate physical significance, and they can be extracted from standard laboratory tests i.e.: the elastic properties of the compact μ and λ in equation (1). Also parameters b_1 and b_2, relative to the Drucker-Prager failure surface in equation (2)-(b), can be obtained via well-established fracture tests, like compression and Brazilian disc tests, on green compacted parts[19] .

Nevertheless, there are other properties, like parameters $s_1(\rho), s_2(\rho)$ in equations (2)-(a) and (3), and the friction coefficient $\mu_d(\rho, \mathrm{v})$ in equation (5) whose evolution in terms of the density ρ and the velocity v cannot be determined by resorting to standard procedures. In Figure 2 to Figure 8, a procedure for that part of the material characterization is sketched. A set of two specimens A (flat) and B, C (open with a large slenderness) is compacted, via a uniaxial single-effect procedure, in an experimental press (developed by AMES S. A.), which is equipped with monitoring and data capturing systems. Two load cells capture the evolution, along the compaction process, of the vertical upper and lower pressures on the specimen and, by resorting to a simple system of pins placed at fixed heights in the die, one or two (depending on the experiment) lateral pressures. In addition, the evolution of the height of the specimen is also registered. The corresponding digitalized histories are captured and recorded in experimental data files. All the specimens were produced using the same Distaloy AE + 0.6% C + 0.6% wax powder blend.

Results for specimen A, with a very small slenderness (Figure 3), are used to extract the compaction properties s_1 and s_2 *assuming* the following hypothesis:

H.1. The stress and the strain fields are homogeneous and independent of the friction effects (due to the small aspect ratio of the specimen).

H.2. The radial component of the plastic strain, e^p_{rr}, is zero (emerging from the hypothesis that the elastic strains are negligible, $\mathbf{e}^e \approx 0$, and that, for this particular geometry, the total radial strain e_{rr} is zero, so that $e^p_{rr} = e_{rr} - e^e_{rr} = -e^e_{rr} \approx 0$).

Under the assumptions above, the evolution equation of the plastic flow, restricted to the radial direction, can be solved for $s_2(P_{ax}, P_{rad})$ in terms of the axial pressure P_{ax} and the radial pressure P_{rad} in Figure 3. In a second step, by substitution into the yield function equation (2)-(a), the evolution of $s_1(P_{ax}, P_{rad})$ can be readily obtained. The specimen density ρ is indirectly measured from the specimen height along the test and the mass M, as indicated in Figure 3. Then, for a given powder mixture to be characterized, $P_{ax}(\rho)$ and $P_{rad}(\rho)$ can be computed. Finally, substitution of these data into those expressions provides the desired evolutions in terms of the density:

$$s_1(\rho) = s_1(P_{ax}(\rho), P_{rad}(\rho)) \quad ; \quad s_2(\rho) = s_2(P_{ax}(\rho), P_{rad}(\rho)) \tag{6}$$

Typical curves $s_1 - \rho$ and $s_2 - \rho$ for iron powder obtained by means of that methodology, are shown in Figure 4.

Once the material properties s_1 and s_2 have been determined from specimen A, results obtained from testing the large slenderness specimen B, C (see Figure 2) are used to extract the friction coefficient $\mu_d(\rho, \mathrm{v})$. Geometrical features of specimens B and C are the same but the corresponding tests differ on the compaction velocity. Specimen B is compacted at the speed $\dot{\delta} = 0.8$ mm./sec. (low compaction speed) and specimen C is compacted at $\dot{\delta} = 8$ mm./sec. (high compaction speed). For these experiments, the following assumptions are done on the friction coefficient:

H.3. The friction coefficient can be split up into two terms:

$$\mu_d(\rho, \mathrm{v}) = \beta(\mathrm{v})\, \kappa(\rho) \tag{7}$$

which uncouple velocity and density dependences in terms of the factors $\beta(\mathrm{v})$ and $\kappa(\rho)$, respectively.

H.4. The normal force t_N, at the powder/die contact cylindrical surface, varies linearly in height.

H.5. The relative velocity powder/die at the contact cylindrical surface has a parabolic variation in height from $\mathrm{v} = 0$ at the bottom of the specimen to $\mathrm{v} = \dot{\delta}$ at the top.

Under those hypothesis, and imposing vertical equilibrium of forces, preliminary analytical solutions for $\beta(\mathrm{v})$ and $\kappa(\rho)$ can be obtained. The corresponding curves $\beta - \mathrm{v}$ and $\kappa - \rho$ are then corrected by comparison of numerical and experimental results in a trial-and-error procedure up to achieve a satisfactory agreement. In Figure 5, typical values of those curves, for an iron powder, are presented.

The values for parameters $s_1(\rho), s_2(\rho)$ and, $\mu_d(\rho, \mathrm{v})$ obtained by means of those procedures *are supposed to hold for the considered powder mixture under any loading conditions in the tested range of densities*, this characterizing the material. In Figure 6 to Figure 8, a comparison between numerical and experimental results for specimens A, B and C, with the

material characterized by the curves in Figure 4 and Figure 5, is presented. There, it can be observed a satisfactory agreement of the numerical results with the experimental measurements.

The characterization curves obtained through the direct calibration procedure presented so far, can only be determined at the range of medium-high densities as the testing machine provides physically meaningful values (typically $[0{,}6-1.0]$ in terms of the relative density). For the low densities range (typically $[0{,}3-0{,}6]$ in terms of the relative density) they could be determined, as a first approximation, by simple extrapolation. This seems to be enough for capturing densification at pure compaction stages. However, preliminary numerical experiments showed that this was not enough as a significant amount of powder transfer takes place. Then, it turns out that, in the low-density range, those material parameters should be determined via a different procedure, *by resorting to indirect measuring of densification effects* on some experimentally measurable physical property, i.e. the transfer ability of the powder. This motivated the experiment presented in next section.

4.1 A powder transfer experiment

As stated above a new set of experiments, to study the material behaviour during the powder transfer stage is required. According to this aim, AMES S.A. designed and built a simple equipment to visualize and measure the powder transfer behaviour. Figure 9 displays a frontal view of this apparatus, where die, core and lower punch can be recognized. The apparatus is equipped with a feed handle that allows the user to move the lower punch to the required positions. In order to observe the internal process the front face of the apparatus is covered with a transparent material.

In Figure 10 a typical initial chamber is presented, where the highlighted L-shaped cavity is filled up with powder through the hole in the upper part of the die. The experiment consists of transferring powder, by means of the motion of the punch, from the L-shaped initial configuration to the upper empty cavity.

In the absence of any type of friction (powder/powder or powder/tooling frictions), one should expect the powder to be transferred to the upper cavity without densification. However, internal and external friction mechanisms lead to local densification and only part of the powder volume lost by the lower L-shaped cavity is transferred to the upper one. Thus, the amount of transferred powder is an indicator of the transfer capability of the mixture and provides an indirect way of calibration for a model aiming at reproducing that effect.

In addition, the apparatus allows a certain control, via the values of h_a and h_b in Figure 10, of the internal and external friction that is mobilized during the experiment and, therefore, of the resulting amount of powder transfer. Experiments in Figure 11 and Figure 12 confirm that assertion: in experiment A the punch is initially placed such that

$h_a = h_b = 20\,mm.(h_a/h_b = 1)$. Then, it is moved up to a final position such that $h_a = 0$ as it is shown Figure 11. There it can be checked that 95% of the initial volume of the lower powder column has been transferred to the final upper column ($b - a = 19$ mm.) and, consequently, little powder densification occurs. This sates that, for this configuration, the mobilized internal and external friction mechanisms are quite small. In experiment B it is set $h_a = 25\,mm.$ and $h_b = 40mm.$ $(h_a/h_b = 0.6)$. The final position of the powder is presented in Figure 12 where it can be seen that just a column of $b - a = 20\,mm.$ (80% of the initial lower column volume) has been transferred. This corresponds to a case of powder transfer involving fairly more densification.

4.2 Calibration of the powder transfer

For the constitutive model in Section 2, powder densification is closely related to the orientation of the normal to the elliptical yield surface, Φ_1 in equation (2)-(a), in the stress space (see Figure 1), which in turn defines the plastic strain flow $\dot{\boldsymbol{\varepsilon}}^p$ for that associative plasticity model (see Figure 13). The higher is the hydrostatic component of $\dot{\boldsymbol{\varepsilon}}^p$ (horizontal component figure) the more compressible is the powder, and the opposite holds for the deviatoric (vertical) component of $\dot{\boldsymbol{\varepsilon}}^p$. It then follows that, for a given path in the stress space during the compaction process (Figure 13-(a)), the flatter is the yield surface the smaller is the resulting compaction (Figure 13-(b)) and the more powder transfer takes place. This is a crucial concept to be exploited for characterization of the powder transfer: *flat elliptical surfaces*, *characterized by small values of the shape factor* s_2 *in equation* (3)*, translate into more powder transfer capacity.*

Parameter s_2 can be then understood as the one that controls the amount of powder transfer and the level of densification during transport of powder and allows focusing that part of powder characterization on determining the $s_2 - \rho$ curve for the low range of densities. In combination with the powder transfer experiments described in Section 4.1., trial and error procedures using the results provided by numerical simulations for different guesses of that curve, allows adjusting the values of s_2 for that low range of densities. In Figure 14, a typical resulting $s_2 - \rho$ curve for the full range of densities, complementing the one obtained for medium-high densities in Figure 2, is presented. Finally, the curve $s_1 - \rho$ for medium-high densities in figure 15 is extrapolated to the low-densities range, this completing the characterization procedure.

5. REPRESENTATIVE NUMERICAL SIMULATIONS

For numerical modelling purposes, POWCOM©, an implicit finite element code for simulation of powder compaction processes, equipped with large strain kinematics, contact-friction algorithms and remeshing strategies, and GID© [18], a customizable graphical pre/post

processor, developed at the International Center for Numerical Methods in Engineering (CIMNE) have been used.

To illustrate the proposed methodology, the powder transfer experiments of Figure 11 and Figure 12 are simulated. Due to the axisymmetric features of the experimental equipment, only 2-D simulations are required. The considered finite-element meshes and initial position of the tools, for both experiments, are shown in Figure 16. They consist of 1422 and 2993 linear triangular elements, respectively, to represent the powder material and the tools. The powder behaviour is simulated by means of the constitutive model described in Section 2, whereas the material parameters are adjusted according to the characterization procedure presented in Section 4. Other values are: apparent density, 3.34 g/cm3, Young's modulus, 300 Mpa, and 0.3 for the Poisson ratio. With no loss of generality, rigid tools are supposed. The considered time interval of the process is 3 seconds divided into 300 time steps.

In Figure 17 and Figure 18 simulation results corresponding to experiments A, in Figure 11, and B, in Figure 12, respectively, are presented. Comparisons in terms of the transferred powder column height and shape (values b and c in the figures) agree, as it should be expected since material characterization was made on that basis. More interestingly, it can be observed as the simulation provides values of non-negligible densifications and non-uniform final density distributions that could affect the simulation of a subsequent compaction process.

6. CONCLUDING REMARKS

Material characterization of powder mixtures at low-density ranges is still an open question. Direct measurements of mechanical properties and densification at those low densities place important experimental difficulties that cannot be easily overcome. On the other hand, numerical modelling of powder transfer in powder compaction processes requires a proper characterization of the powder densification at low densities.

Throughout the preceding sections, a methodology for calibration of powder transfer in compaction processes has been presented. Based on a simple apparatus, simple experiments provide measurable results in terms of powder transfer, which can be used to indirect material characterization of powder mixtures at low densities ranges for specific constitutive models. This complements classical material characterization procedures for medium-high density ranges. Examples of application to a particular constitutive model have been provided.

The proposed methodology appears to be simple and industrially viable. As it is applied to the specific constitutive model used by the authors, allows direct determination of the specific parameter that defines the aspect ratio of the elliptical cup surface which, in turn, is responsible for the amount of densification in powder transfer processes. It seems that this methodology could also be applied to other families of constitutive models for powder

compaction. As a relevant result, this would allow the same constitutive model to be used, via only the appropriated material characterization, for simulation of densification in powder transfer stages as well as in pure compaction stages.

ACKNOWLEDGMENTS

Support of the Spanish "Ministerio de Ciencia y Tecnología" (MCYT) under grants no. MAT2000-0436 and DPI2001-2256-C02-02, is gratefully acknowledged.

REFERENCES

[1] B. Aren, A. Nilsson: Powder Metall. **30**, 1987, 87-96.
[2] S. Brown and G. Weber: 'A Constitutive Model for the Compaction of Metal Powders', Dep. Mat. Science and Eng. MIT, Cambridge, MA, 02139, 1988.
[3] D. T. Gethin, and R. W. Lewis: Proc. Powder Metallurgy world Congress, 1994.
[4] R. Ransing, I. Cameron, N. Lavery, A. Khoei, R. Lewis, and D. Gethin: Proc. International Workshop on Modelling of Metal Powder Forming Processes, Grenoble, France 21-23 July 1997.
[5] A. K. Ariffin, D. T. Gethin, and R. W. Lewis: Powder Metall.,1998, **41**,3, 189-197.
[6] A.R Khoei and R.W. Lewis: Int. J. Numer. Methods Eng. 1999, **45**, 801-820.
[7] W. A. M. Brekelmans, J. D. Janssen and A. A. F. Van De Ven and G. de With: Int. J. Num. Methods. Eng. **31**, 509-524, 1991.
[8] T. Nakagawa and M. Sato: Proc. Powder Metallurgy World congress, Vol. 2, 1992.
[9] J. C. Cante: 'Simulación numérica de procesos de compactación de pulvimateriales', PhD thesis, UPC, Spain, 1995.
[10] J. Oliver, S. Oller, J. C. Cante: Int. J. Solids and Struct, **33**, 3161-3178, 1996.
[11] Weyler Rafael: 'Simulación numérica de procesos de compactación y extrusión de materiales pulverulentos', PhD thesis, UPC, Spain, 2000.
[12] J. Oliver, J. C. Cante, J.A. Bas, A. Bolarin: Proc. Powder Metallurgy world Congress, 1998, Granada, Spain.
[13] P. Brewin, P. Doremus, D. T. Gethin, P. Skoglund, J. H. tweed, and H. Wiedemann: Proc. Review EU thematic network, Powder Metallurgy World congress, 2000.
[14] E. Pavier : 'Caracterisation du comportament d'une poudre de fer pour le procede de compression en matrice', PhD, L'Institut National Polytechnique, grenoble, France,1992.
[15] PM Modnet Methods and Measurements Group: Powder Metall., **43**, No. 4, 364-674, 2000.
[16] PM Modnet Computer Modelling Group: Powder Metall, **42**, No. 4, 301-311, 1999.
[17] PM Modnet Research Group: Powder Metall., 2002, **45**, 335-344.

[18] GID. ´The customizable pre and post-processor', International Center for Numerical Methods in Engineering (CIMNE), http://www.cimne.upc.es, 2003
[19] P. Doremus, F. Toussaint, and O. Alvain : in 'Recent developments in computer modelling of powder metallurgy processes',NATO Advanced Research Workshop, Seies III : Computer and Systems Science, (eds. A. Zavaliangos and A. Laptev), Vol. 176, 29-41;2001,Amsterdam, IOS press
[20] Chuan-Yu Wu, Alan C.F. Cocks and Olivier T. Gillia. Experimental and Numerical Investigation of filling and Powder Transfer - Advances in Powder Metallurgy and Particulate Materials, 4, 2002, p.258-272
[21] Chuan-Yu Wu, Luiza Dihoru, Alan C.F. Cocks. The Flow of Powder into Simple and Complex Shaped Dies: Powder Technology, 134, 2003, p.24-39
[22] Lee, E.H. and Liu, D.T. Finite Strain Elastic-Plastic Theory Particulary for Plane Wave analysis. J. Appl. Phhys., 38

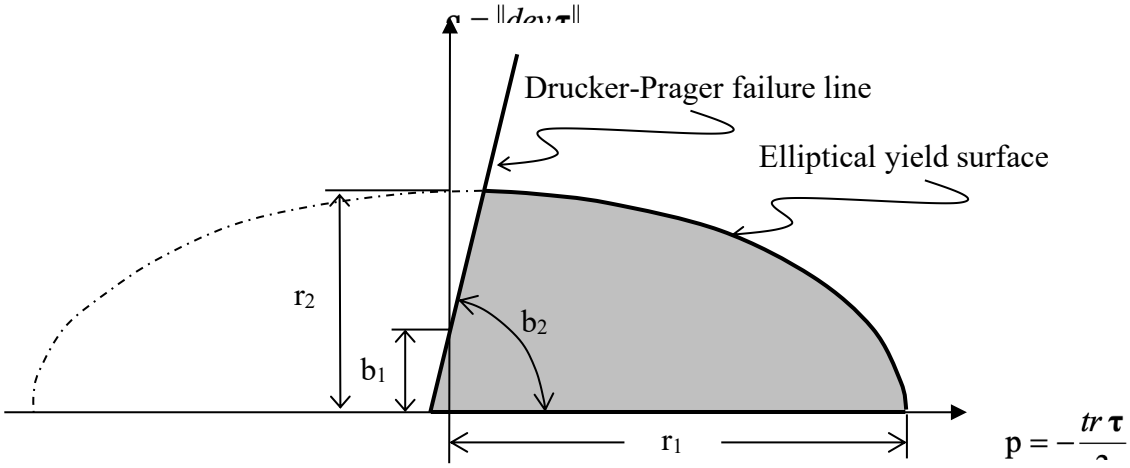

Figure 1: Yield surface: centred ellipse and Drucker- Prager line

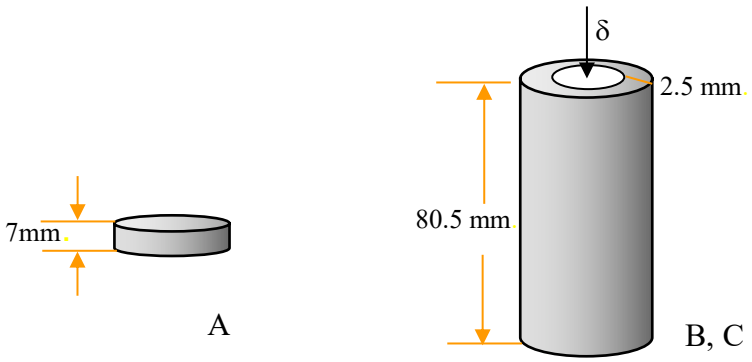

Figure 2: Specimens for material characterization. Specimen A (slenderness height/radius ≈ 1) and specimens B, C (slenderness height/thickness ≈ 17-30)

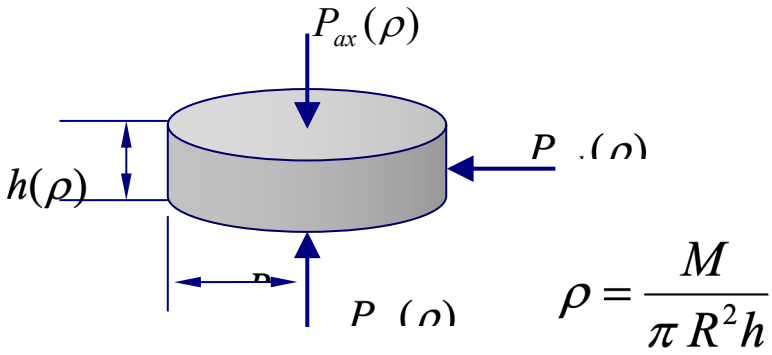

Figure 3: Low slenderness specimen

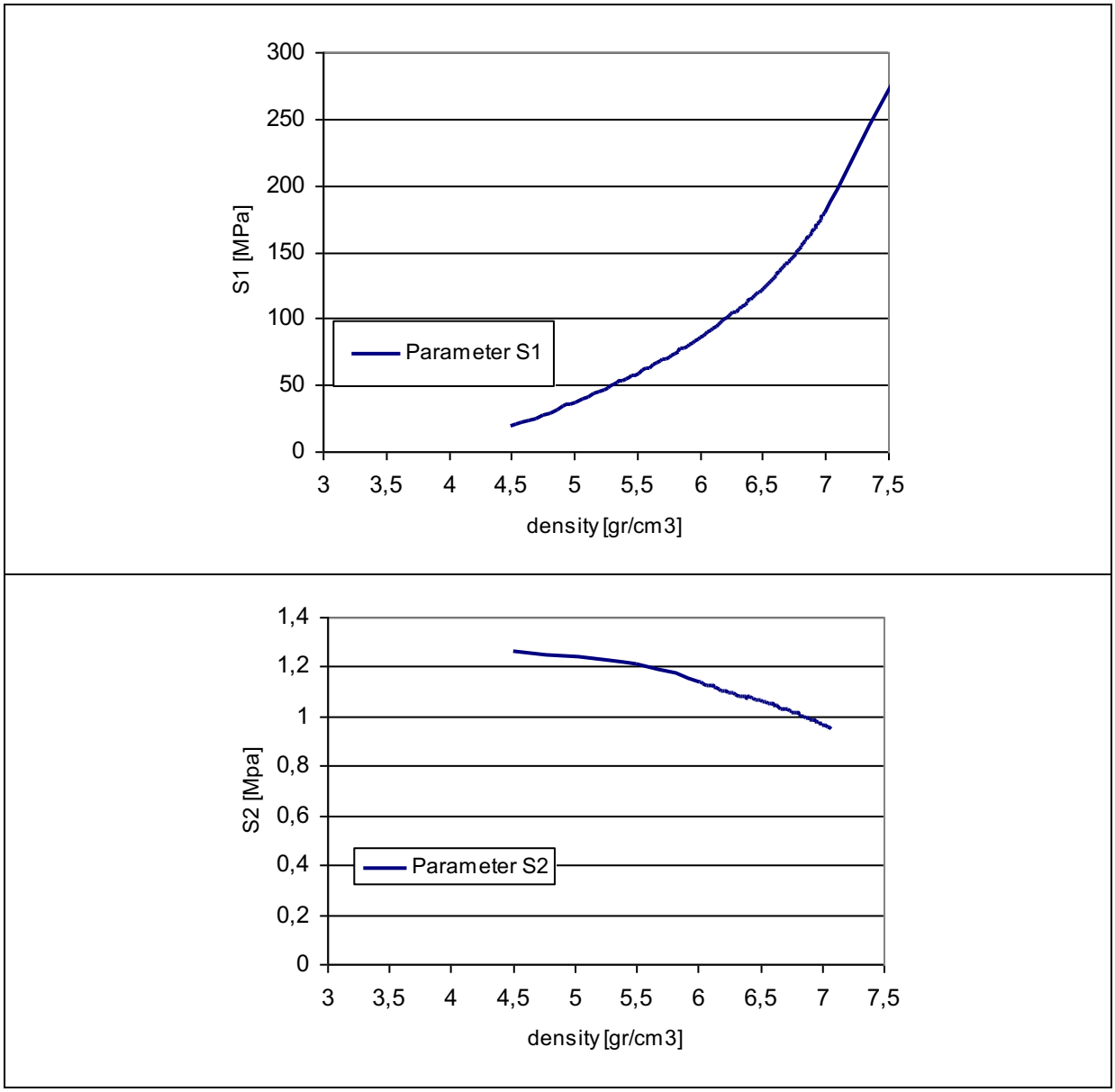

Figure 4: Evolution of parameters s_1 and s_2 in terms of the density

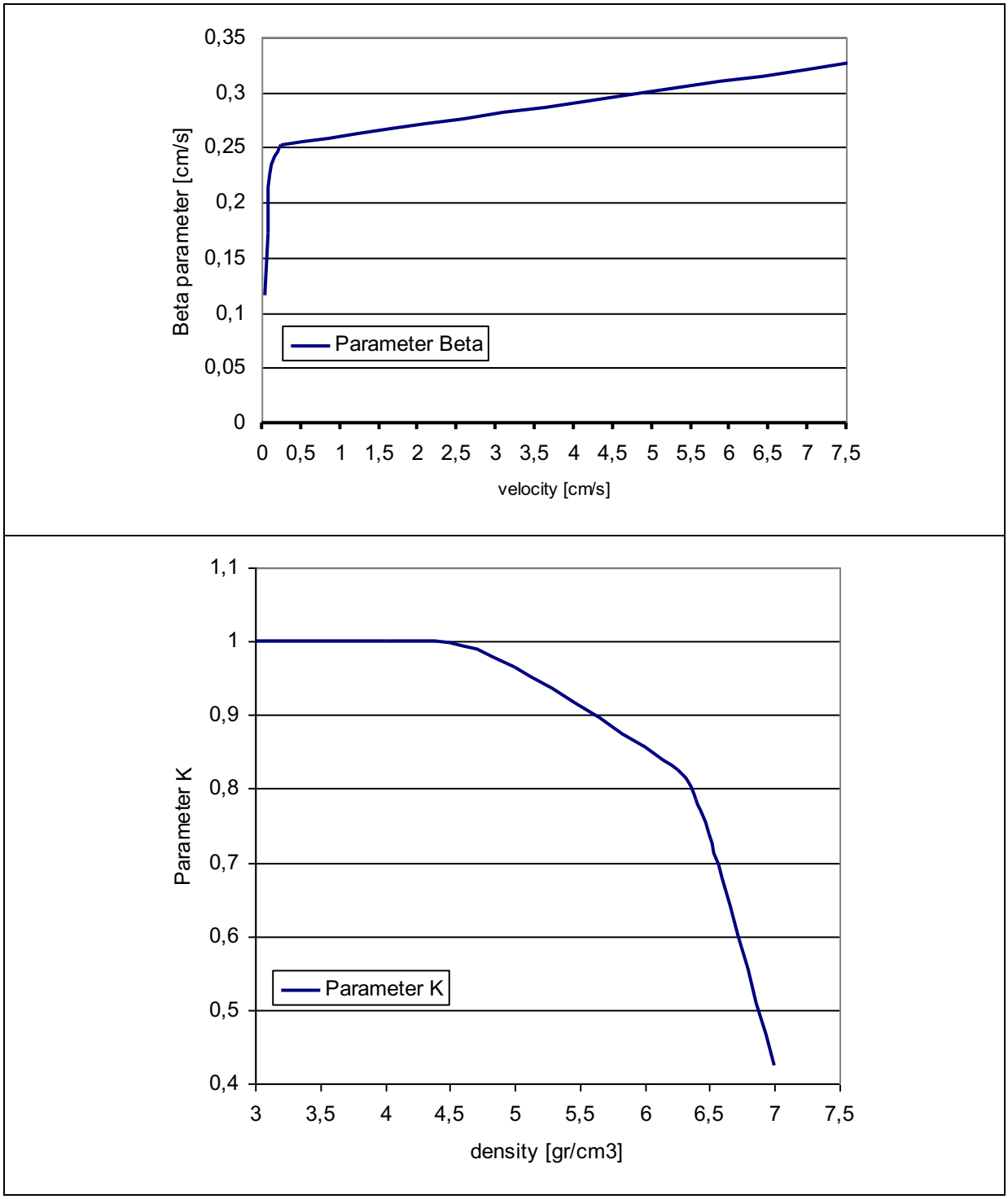

Figure 5: Evolution of $\beta(\mathrm{v})$ and $\kappa(\rho)$

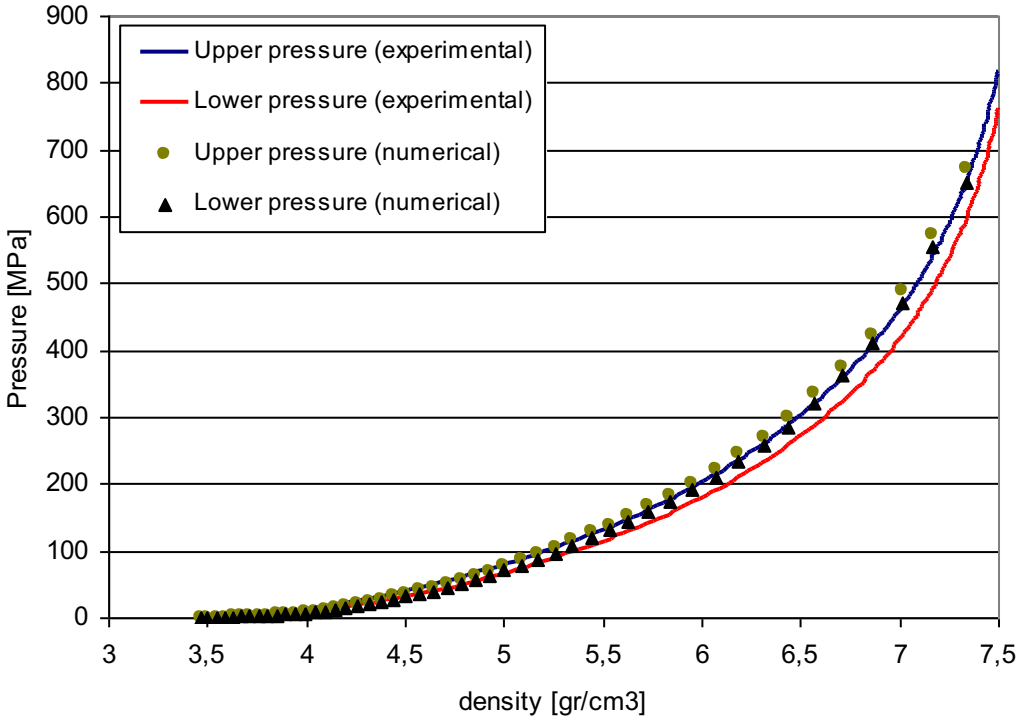

Figure 6: Uniaxial compaction of a low slenderness part. Specimen A.

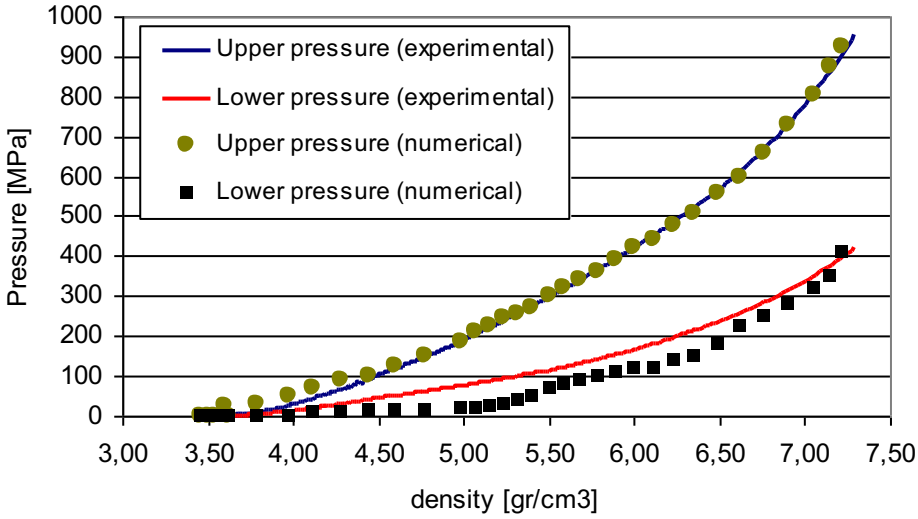

Figure 7: Uniaxial compaction of a high slenderness part. Specimen B ($\dot{\delta}$ = 0.8 mm/s)

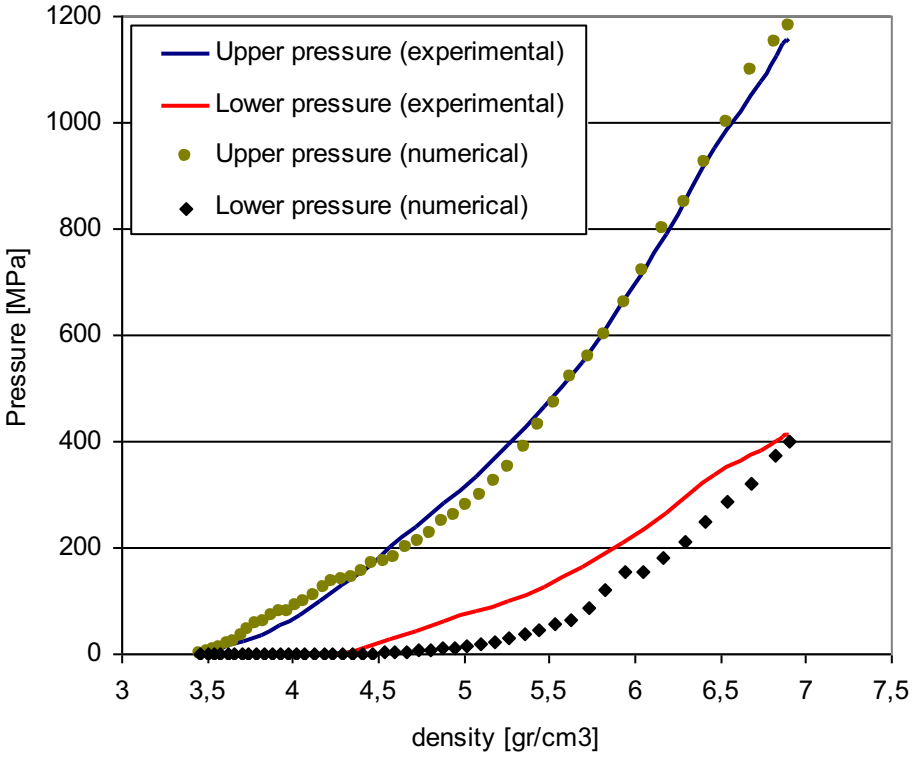

Figure 8: Uniaxial compaction of a high slenderness part. Specimen C ($\dot{\delta}$ = 8 mm/s)

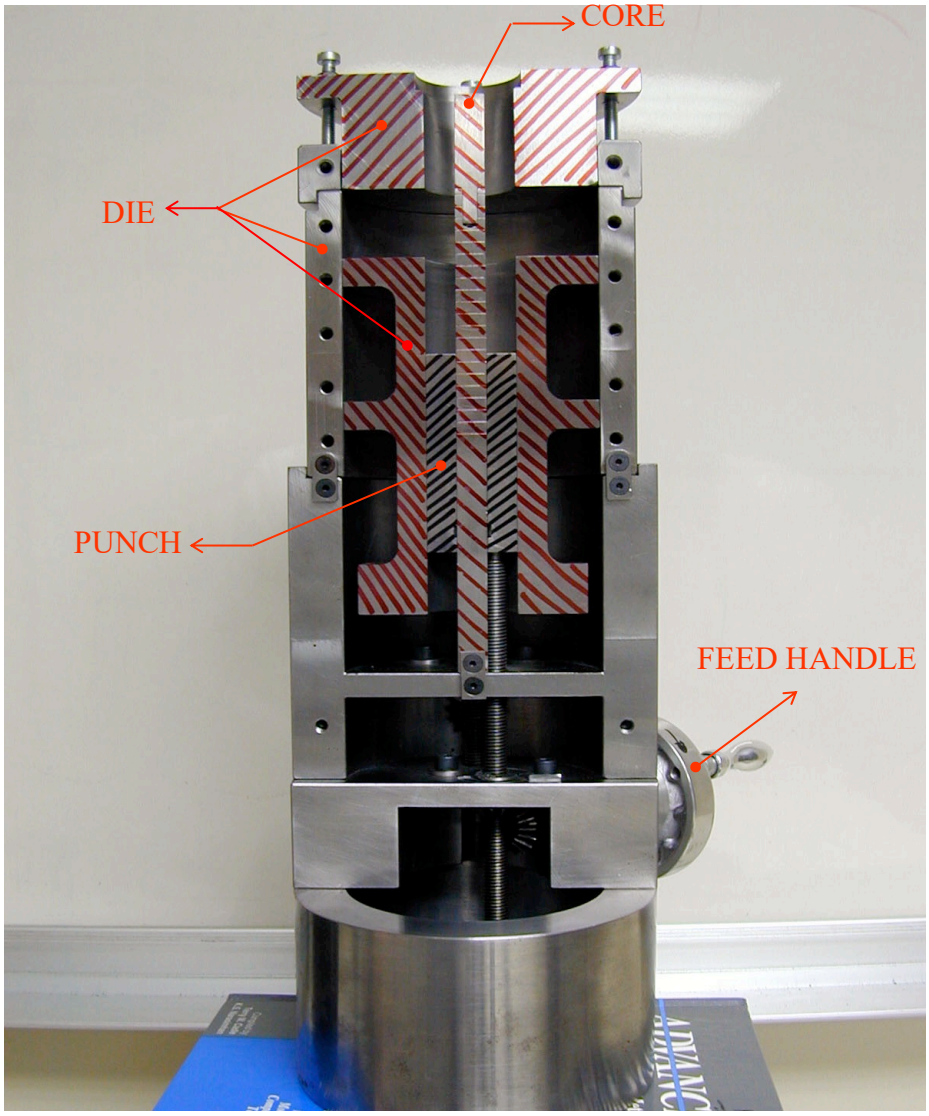

Figure 9: Specific apparatus to study the powder transfer

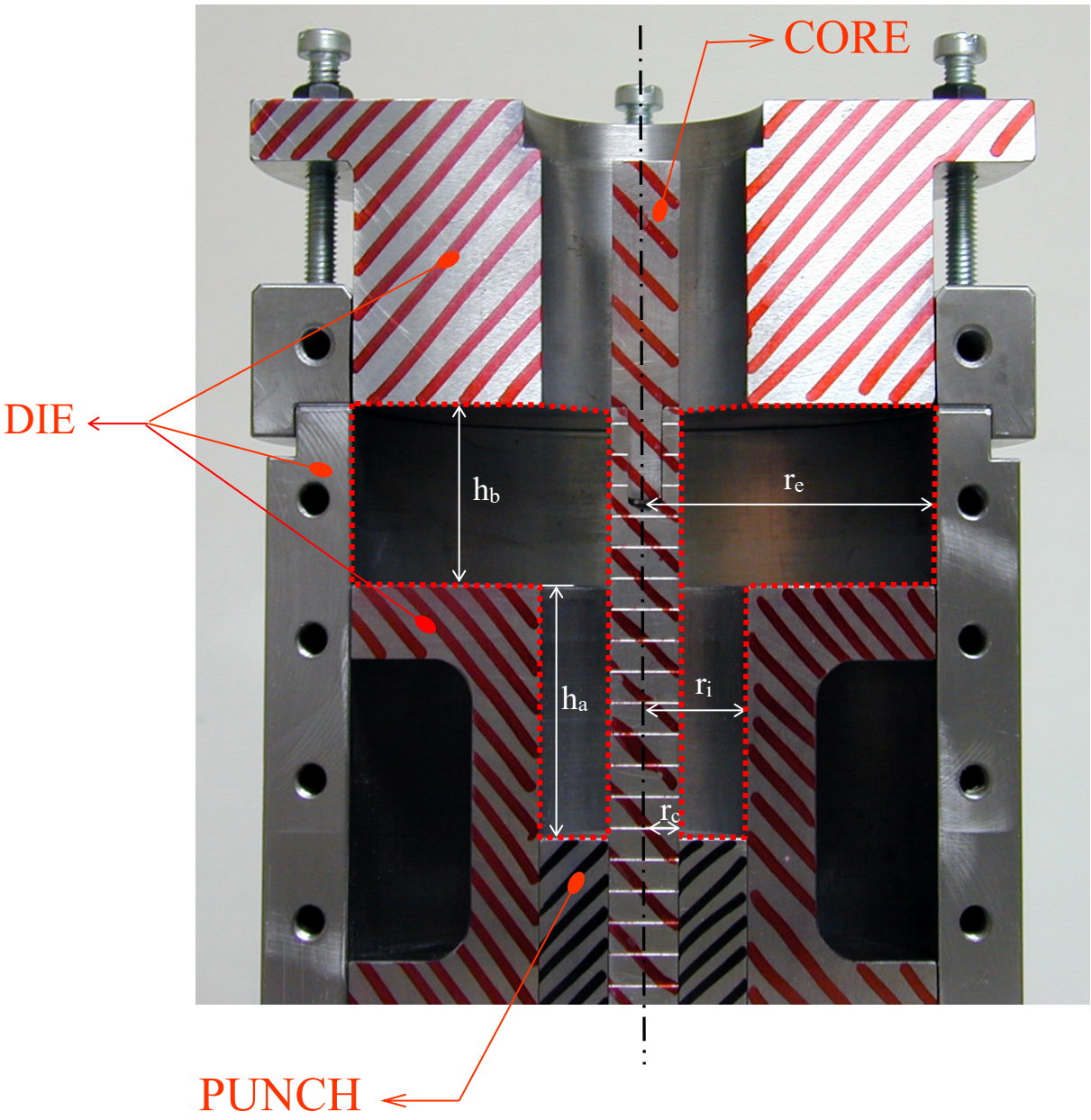

Figure 10: Frontal view of the initial chamber. r_e = 51mm, r_i = 18mm, r_c = 6mm

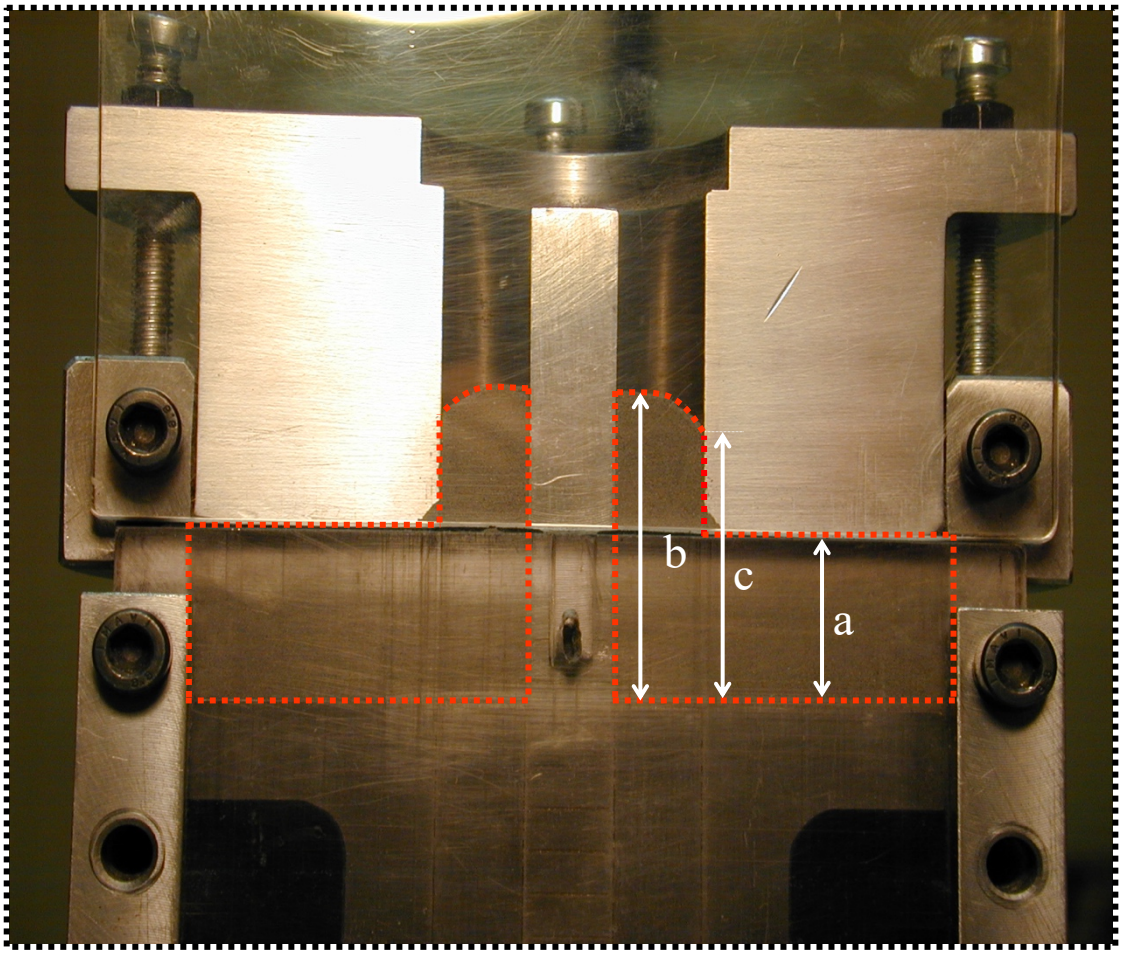

Figure 11: Experiment A: final deformation of the powder after the transfer stage.
Lower punch displacement is 20 mm.
a = 20 mm., b = 39 mm. and c = 35 mm.

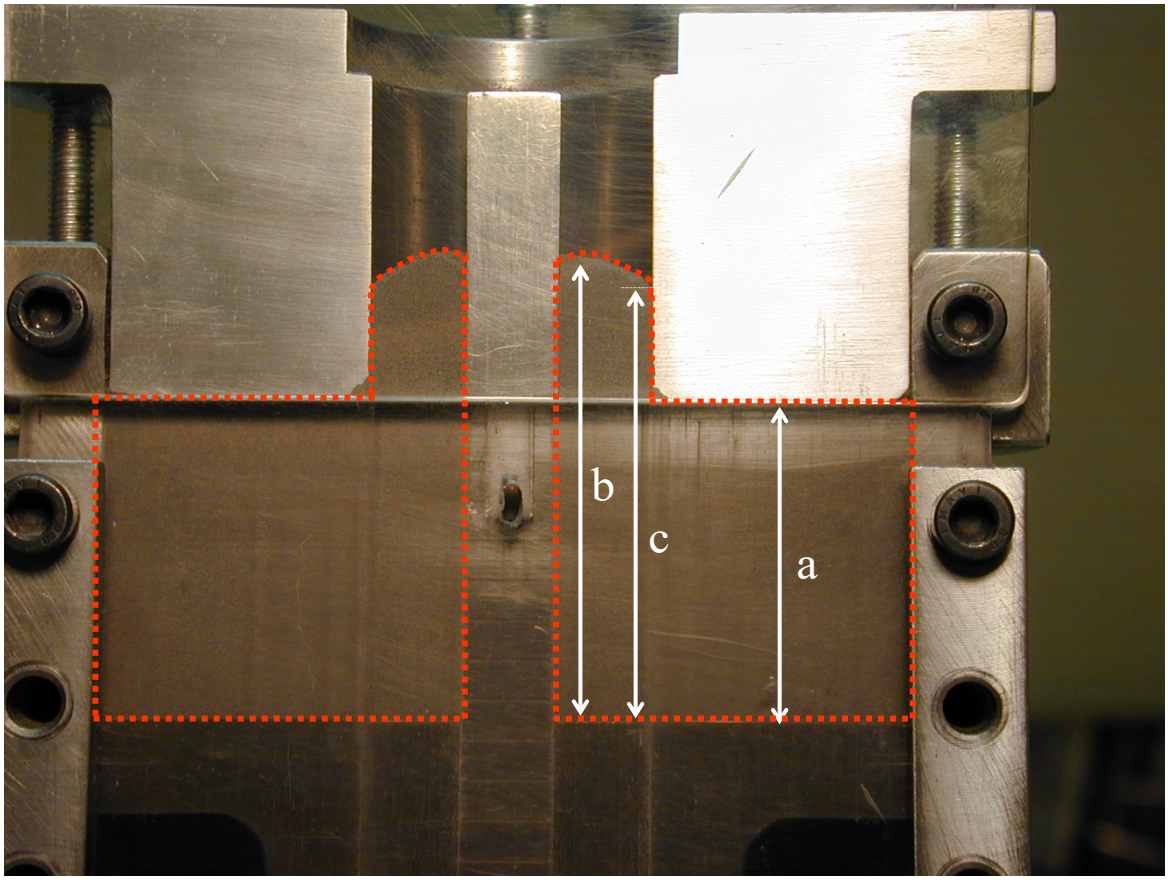

Figure 12: Experiment B: final position of the powder after the transfer stage.
Lower punch displacement is 25 mm.
a = 40 mm., b = 60 mm. and c = 54 mm.

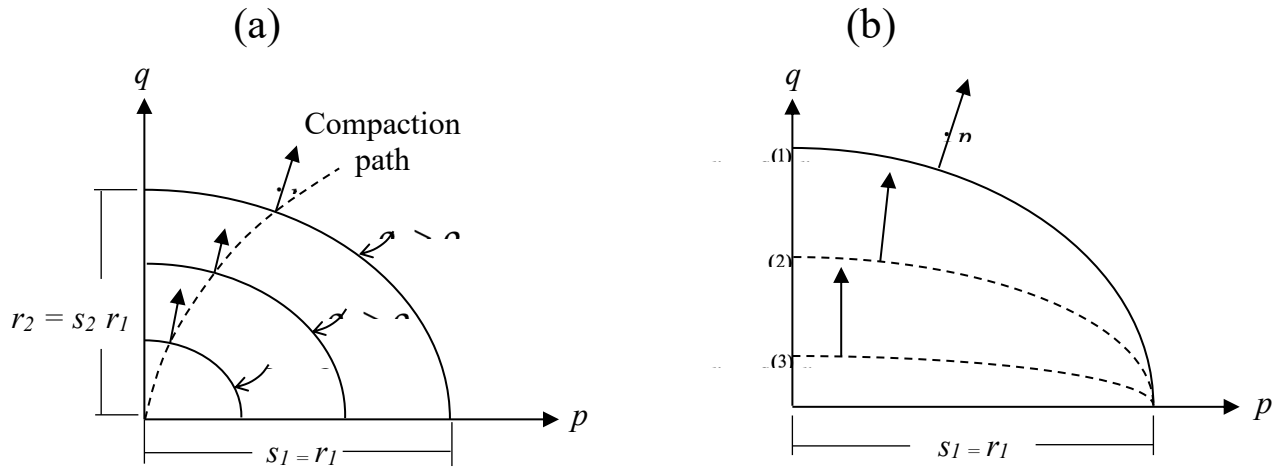

Figure 13: (a) Typical yield surface shape and plastic flow vector for a compaction process. (b) Yield surface and plastic flow vector for different values of the shape factor s_2

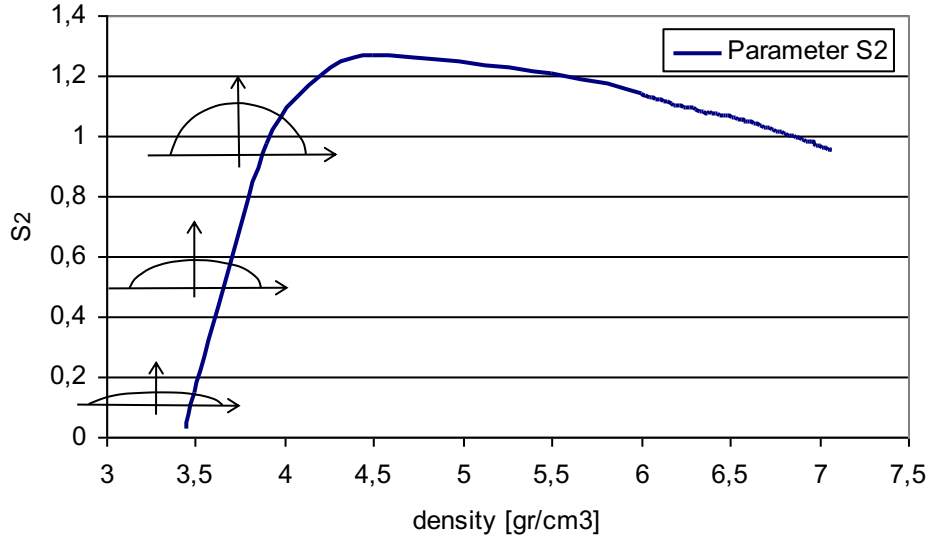

Figure 14: Typical $s_2 - \rho$ curve for the complete range of densities

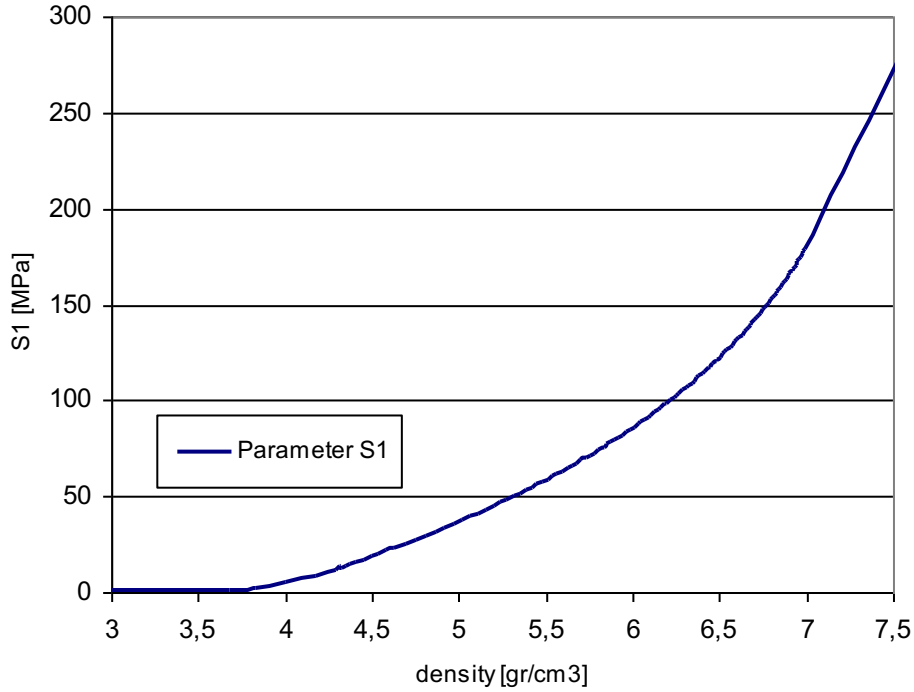

Figure 15: Typical $s_1 - \rho$ curve for the complete range of densities

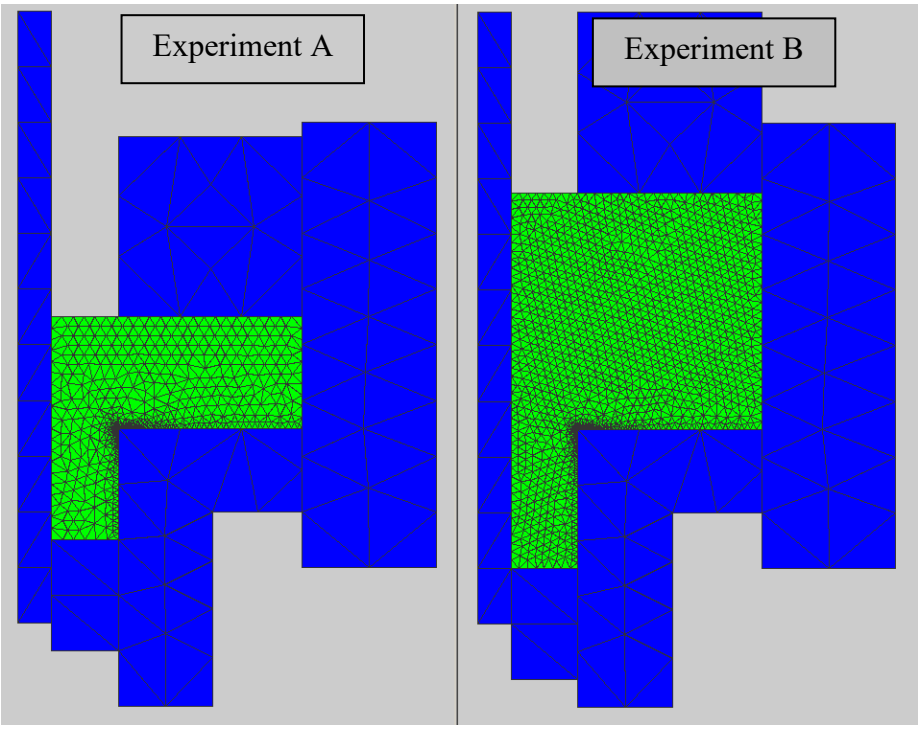

Figure 16: Numerical simulation of powder transfer experiments A and B. Initial geometries and finite element meshes.

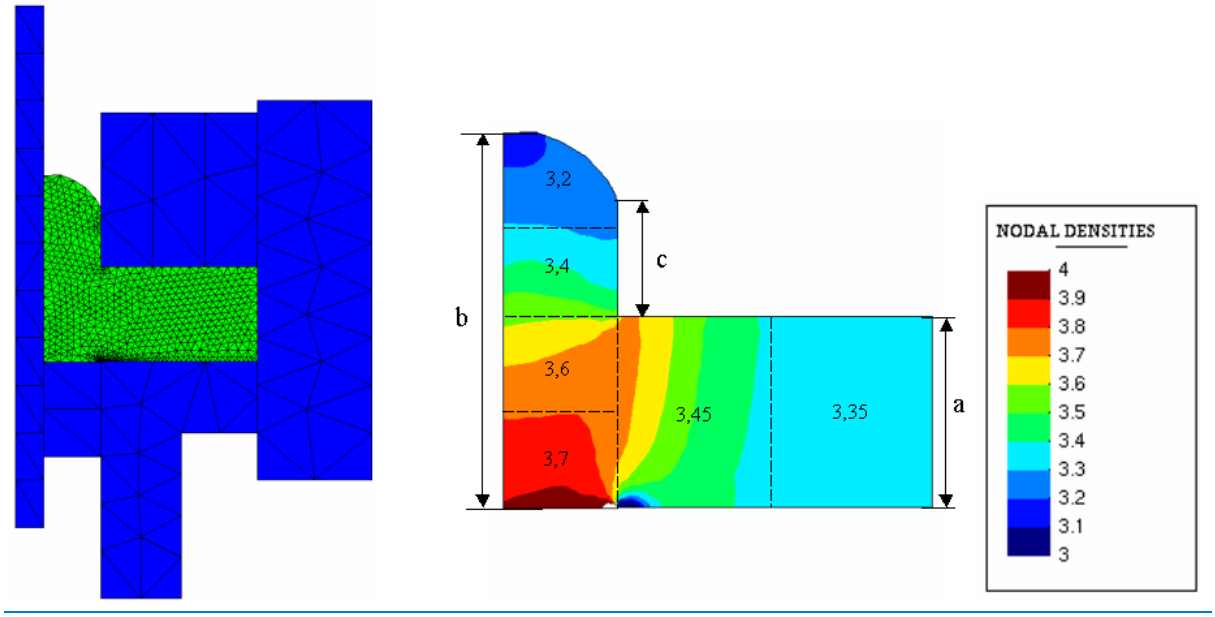

Figure 17: Numerical results for powder transfer experiment A in Figure 11.
Final powder position and density distribution.
a = 20 mm., b = 39mm. and c = 12 mm

.

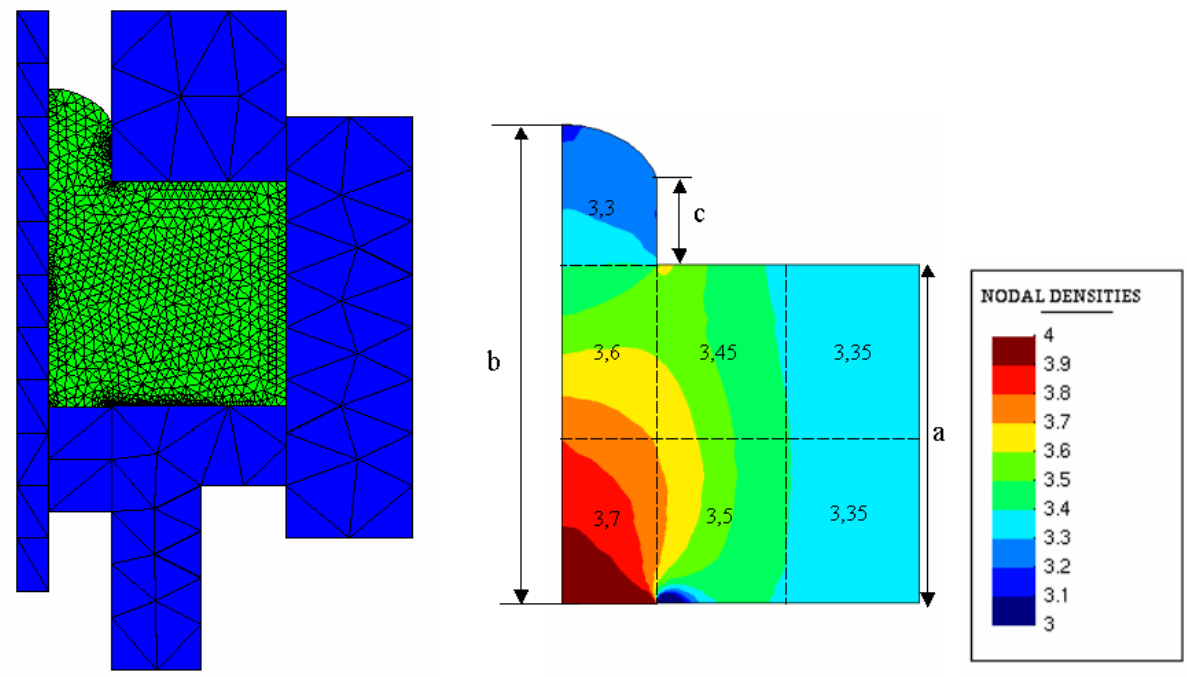

Figure 18: Numerical results for powder transfer experiment B in Figure 12.
Final powder position and density distribution.
a = 40 mm., b = 60mm. and c = 11 mm.